University of Groningen

Measurement of e+e− → ωη′ cross sections at s = 2.000 to 3.080 GeV

BESIII Collaboration; Ablikim, M.; Achasov, M. N.; Adlarson, P.; Ai, X. C.; Aliberti, R.; Amoroso, A.; Kalantar-Nayestanaki, N.; Kappert, R.; Kavatsyuk, M.

Published in:
Journal of High Energy Physics

DOI:
10.1007/JHEP07(2024)093

IMPORTANT NOTE: You are advised to consult the publisher's version (publisher's PDF) if you wish to cite from it. Please check the document version below.

Document Version
Publisher's PDF, also known as Version of record

Publication date:
2024

Link to publication in University of Groningen/UMCG research database

Citation for published version (APA):
BESIII Collaboration, Ablikim, M., Achasov, M. N., Adlarson, P., Ai, X. C., Aliberti, R., Amoroso, A., Kalantar-Nayestanaki, N., Kappert, R., Kavatsyuk, M., Messchendorp, J., & Rodin, V. (2024). Measurement of e+e− → ωη′ cross sections at s = 2.000 to 3.080 GeV. *Journal of High Energy Physics*, *2024*(7), Article 93. https://doi.org/10.1007/JHEP07(2024)093

Copyright
Other than for strictly personal use, it is not permitted to download or to forward/distribute the text or part of it without the consent of the author(s) and/or copyright holder(s), unless the work is under an open content license (like Creative Commons).

The publication may also be distributed here under the terms of Article 25fa of the Dutch Copyright Act, indicated by the “Taverne” license. More information can be found on the University of Groningen website: https://www.rug.nl/library/open-access/self-archiving-pure/taverne-amendment.

Take-down policy
If you believe that this document breaches copyright please contact us providing details, and we will remove access to the work immediately and investigate your claim.

Downloaded from the University of Groningen/UMCG research database (Pure): http://www.rug.nl/research/portal. For technical reasons the number of authors shown on this cover page is limited to 10 maximum.

Download date: 03-11-2024

Published for SISSA by Springer

Received: *April 12, 2024*
Accepted: *June 26, 2024*
Published: *July 10, 2024*

Measurement of $e^+e^- \to \omega\eta'$ cross sections at $\sqrt{s} = 2.000$ to 3.080 GeV

The BESIII collaboration

E-mail: besiii-publications@ihep.ac.cn

Abstract: We measured the Born cross sections for the process $e^+e^- \to \omega\eta'$ at 22 center-of-mass energies from 2.000 to 3.080 GeV with the BESIII detector at the BEPCII collider. We observed a resonant structure with a statistical significance of 9.6σ. A Breit-Wigner fit determines its mass to be $M_R = (2153 \pm 30 \pm 31)\,\mathrm{MeV}/c^2$ and its width to be $\Gamma_R = (167 \pm 77 \pm 7)\,\mathrm{MeV}$, where the first uncertainties are statistical and the second are systematic.

Keywords: e^+-e^- Experiments, Particle and Resonance Production, Spectroscopy

ArXiv ePrint: 2404.07436

https://doi.org/10.1007/JHEP07(2024)093

Contents

1 Introduction

Hadron spectroscopy offers valuable insights into the non-perturbative dynamics of the strong interaction and has caught the attention of both theorists and experimentalists. According to the Particle Data Group (PDG) [1], there are several vector states of the ω family around 2.2 GeV, i.e., $\omega(2220)$, $\omega(2290)$ and $\omega(2330)$, which need to be confirmed. It is noteworthy that the measured widths are usually at least twice as wide as the theoretical calculations [2–7]. The experimental measured parameters are summarized in table 1.

The BaBar Collaboration has studied the process $e^+e^- \to \omega\pi^+\pi^-$ using the initial state radiation (ISR) method. The cross section line shape shows evidence for an isoscalar resonance structure near 2.25 GeV with a significance of 2.6σ [8, 9]. The BESIII Collaboration has studied the processes $e^+e^- \to \omega\eta$ [10], $e^+e^- \to \omega\pi^0\pi^0$ [11] and $e^+e^- \to \omega\pi^+\pi^-$ [12] at center-of-mass (c.m.) energies ($\sqrt{s}$) from 2.000 to 3.080 GeV. Two enhanced structures around 2.2 GeV are observed with resonance parameters $M_1 = 2176 \pm 24$ MeV/c^2, $\Gamma_1 = 89 \pm 50$ MeV and $M_2 = 2232 \pm 19$ MeV/c^2, $\Gamma_2 = 93 \pm 53$ MeV, respectively. The authors in reference [13] introduced the $\omega(4S)$ and $\omega(3D)$ to represent the behavior of these enhanced structures, and claimed that these two structures are caused by the interference of $\omega(4S)$ and $\omega(3D)$. To establish higher excited ω states, more theoretical and experimental efforts are desirable.

Particle	Mass (MeV/c^2)	Width (MeV)	Channel
$\omega(2220)$	2232 ± 33	90 ± 60	$e^+e^- \to \omega\pi^+\pi^-$ $e^+e^- \to \omega\pi^0\pi^0$
$^*\omega(2290)$	2290 ± 20	275 ± 35	$p\bar{p} \to \Lambda\bar{\Lambda}$
$^*\omega(2330)$	2330 ± 30	435 ± 75	$\gamma p \to \rho^\pm\rho^0\pi^\mp$

Table 1. Possible 1^{--} ω states and their parameters, while * denotes further states observed by a single group or states poorly established that thus need confirmation.

In this paper, we present a measurement of the Born cross sections for the process $e^+e^- \to \omega\eta'$ at $\sqrt{s}$ from 2.000 to 3.080 GeV based on 22 data samples corresponding to an integrated luminosity of 650 pb^{-1} collected by the BESIII experiment.

2 BESIII detector and Monte Carlo simulation

The BESIII detector [14] records symmetric e^+e^- collisions provided by the BEPCII storage ring [15] in the range of $\sqrt{s}$ from 2.0 to 4.95 GeV, with a peak luminosity of 1×10^{33} $\mathrm{cm}^{-2}\mathrm{s}^{-1}$ achieved at $\sqrt{s} = 3.77$ GeV. BESIII has collected large data samples in this energy region [16]. The cylindrical core of the BESIII detector covers 93% of the full solid angle and consists of a helium-based multilayer drift chamber (MDC), a plastic scintillator time-of-flight system (TOF), and a CsI(Tl) electromagnetic calorimeter (EMC), which are all enclosed in a superconducting solenoidal magnet providing a 1.0 T (0.9 T in 2012) magnetic field. The solenoid is supported by an octagonal flux-return yoke with resistive plate counter muon identification modules interleaved with steel. The charged-particle momentum resolution at 1 GeV/c is 0.5%, and the specific ionization energy loss ($\mathrm{d}E/\mathrm{d}x$) resolution is 6% for electrons from Bhabha scattering. The EMC measures photon energies with a resolution of 2.5% (5%) at 1 GeV in the barrel (end cap) region. The time resolution in the TOF barrel region is 68 ps, while that in the end cap region is 110 ps.

Simulated data samples produced with a GEANT4-based [17] Monte Carlo (MC) package, which includes the geometric description [18] of the BESIII detector and the detector response, are used to optimize the event selection criteria, estimate background processes, and determine the detection efficiency. The signal MC samples for the process $e^+e^- \to \omega\eta'$ are generated by ConExc [19] so that the contribution of the P-wave amplitude between the vector and pseudoscalar mesons in the final state is taken into account. The η' and ω are reconstructed by $\gamma\pi^+\pi^-$ and $\pi^+\pi^-\pi^0$ mode, respectively. The decay of the η' and ω are described by the observed amplitude patterns in $\eta' \to \gamma\pi^+\pi^-$ and $\omega \to \pi^+\pi^-\pi^0$, respectively [20, 21]. For background studies, MC samples of inclusive hadronic events are generated with a hybrid generator that integrates ConExc [19], LUARLW [22] and PHOKHARA [23]. Exclusive MC samples of $e^+e^- \to \omega\pi^+\pi^-$ and $e^+e^- \to 2(\pi^+\pi^-\pi^0)$ are generated by ConExc [19] according to published results of BESIII and BaBar [12, 24].

3 Event selection and background analysis

The signal process $e^+e^- \to \omega\eta'$ is reconstructed using $\omega \to \pi^+\pi^-\pi^0$, $\pi^0 \to \gamma\gamma$ and $\eta' \to \gamma\pi^+\pi^-$. The signal candidates are required to have four charged pions with zero net charge and at least three photons.

Charged tracks detected in the MDC are required to be within a polar angle (θ) range of $|\cos\theta| < 0.93$, where θ is defined with respect to the z axis, which is the symmetry axis of the MDC. For each charged track, the distance of closest approach to the interaction point (IP) is required to be within 10 cm in the beam direction and within 1 cm in the plane perpendicular to the beam direction. Particle identification (PID) for charged tracks combines measurements of the $\mathrm{d}E/\mathrm{d}x$ in the MDC and the flight time in the TOF to form likelihoods $\mathcal{L}(h)(h = p, K, \pi)$ for each hadron h hypothesis. Charged tracks are identified as pions when the pion hypothesis has the greatest likelihood [$\mathcal{L}(\pi) > \mathcal{L}(K)$ and $\mathcal{L}(\pi) > \mathcal{L}(p)$].

Photon candidates are identified using isolated showers in the EMC. The deposited energy of each shower must be more than 25 MeV in the barrel region ($|\cos\theta| < 0.80$) and more than 50 MeV in the end cap region ($0.86 < |\cos\theta| < 0.92$). To exclude showers that originate from charged tracks, the angle subtended by the EMC shower and the position of the closest charged track at the EMC must be greater than 10° as measured from IP. To suppress electronic noise and showers unrelated to the event, the difference between the EMC time and the event start time of the photon candidate is required to be within [0,700] ns.

To suppress the background and improve kinematic resolution, a four-constraint (4C) kinematic fit imposing energy-momentum conservation is carried out under the hypothesis of $e^+e^- \to 2(\pi^+\pi^-)3\gamma$. If there are more than three photons in one event, the combination with the minimum $\chi^2_{4\mathrm{C}}$ is retained for further analysis. The candidate events are required to satisfy $\chi^2_{4\mathrm{C}} < 60$. Kinematic fit improves signal purity from 7.3% to 41.5%. To suppress the contamination from the $e^+e^- \to 2(\pi^+\pi^-)\pi^0$ or $e^+e^- \to 2(\pi^+\pi^-\pi^0)$ processes, two additional 4C kinematic fits under the hypotheses of $e^+e^- \to 2(\pi^+\pi^-\gamma)$ and $e^+e^- \to 2(\pi^+\pi^-2\gamma)$ are independently performed. Only those events which satisfy $\chi^2_{4\mathrm{C}} < \chi^2_{4\mathrm{C}}(2(\pi^+\pi^-\gamma))$ and $\chi^2_{4\mathrm{C}} < \chi^2_{4\mathrm{C}}(2(\pi^+\pi^-2\gamma))$ are retained. The photon combination with the smallest value of $|M(\gamma\gamma) - M_{\pi^0}|$ is assigned as the π^0, where M_{π^0} is the π^0 known mass [1]. The distribution of $\gamma\gamma$ invariant mass, $M(\gamma\gamma)$, at $\sqrt{s} = 2.125$ GeV is shown in figure 1(a). The ω candidate is assigned to the $\pi^+\pi^-\pi^0$ combination with the smallest value of $|M(\pi^+\pi^-\pi^0) - M_\omega|$, where M_ω is the ω known mass [1]. The distribution of $\pi^+\pi^-\pi^0$ invariant mass, $M(\pi^+\pi^-\pi^0)$, at $\sqrt{s} = 2.125$ GeV is shown in figure 1(b). The distribution of the invariant mass of the remaining photon and $\pi^+\pi^-$, $M(\gamma\pi^+\pi^-)$, at $\sqrt{s} = 2.125$ GeV is shown in figure 1(c), where an η' signal is visible with the $|M(\gamma\gamma) - M_{\pi^0}| < 0.015\,\mathrm{GeV}/c^2$ and $|M(\pi^+\pi^-\pi^0) - M_\omega| < 0.029\,\mathrm{GeV}/c^2$ requirements, corresponding to about 3σ in the mass resolutions. The signal region of the η' is defined as $|M(\gamma\pi^+\pi^-) - M_{\eta'}| < 0.025$ GeV$/c^2$, where $M_{\eta'}$ is the η' known mass [1]. The sideband region of the η' is defined as $0.05 < |M(\gamma\pi^+\pi^-) - M_{\eta'}| < 0.10$ GeV$/c^2$.

After applying the above requirements, the background that still exists. We studied the remaining potential background sources by analyzing inclusive $e^+e^- \to$ hadrons and exclusive MC samples. Exclusive MC samples for $e^+e^- \to \omega\pi^+\pi^-$ and $e^+e^- \to 2(\pi^+\pi^-\pi^0)$ are generated by ConExc [19] with a DIY amplitude model introduced in ref. [12] for the process $e^+e^- \to \omega\pi^+\pi^-$ and a phase-space model for the process $e^+e^- \to 2(\pi^+\pi^-\pi^0)$ taking into account the cross sections measured by BaBar [24]. Simulated events are subject to the same selection procedure as the signal process. Those non-η' events, e.g., $e^+e^- \to \omega\pi^+\pi^-$, form a peaking background in the $M(\pi^+\pi^-\pi^0)$ distribution, as shown in figure 1(b) and are estimated using the η' sideband. The background in the $M(\gamma\pi^+\pi^-)$ distribution, determined from exclusive MC samples and the inclusive hadronic MC sample, is flat. Therefore, the number of signal is determined by fitting the $M(\gamma\pi^+\pi^-)$ spectrum. The dominant background stems from the $e^+e^- \to 2(\pi^+\pi^-\pi^0)$ process. The background distribution obtained from the inclusive hadronic MC sample, which has been normalized to the integrated experimental luminosity, is shown in figure 1(c).

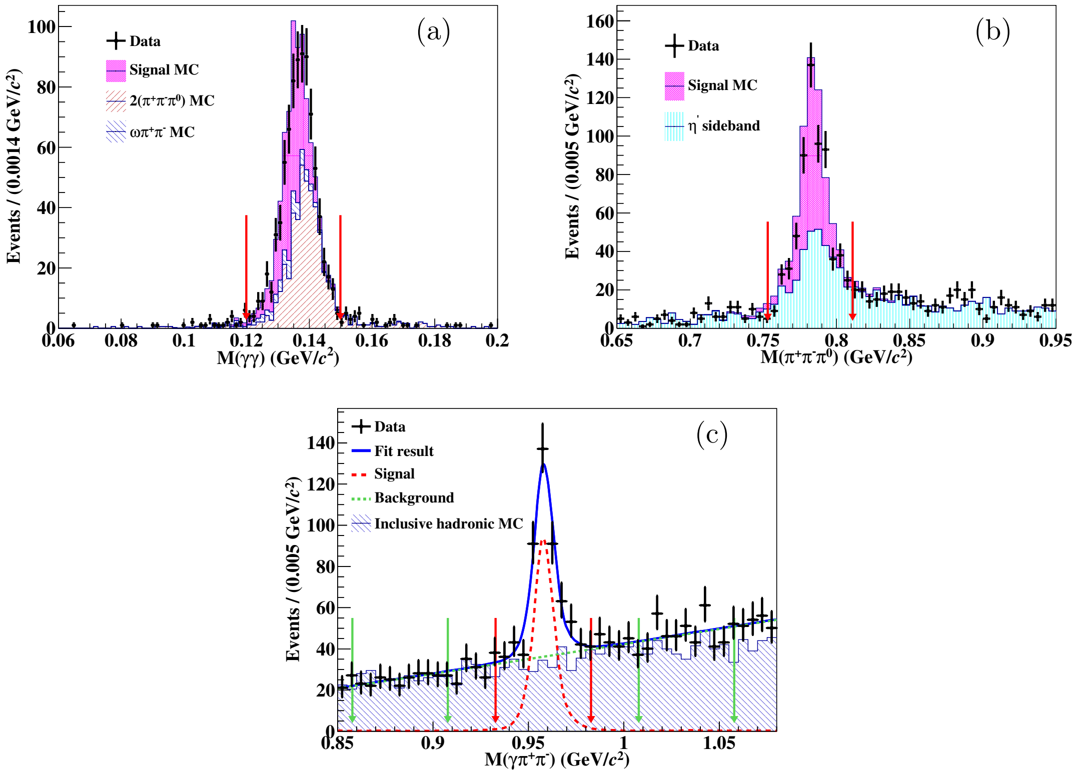

Figure 1. (a) Distribution of $M(\gamma\gamma)$, where the (black) dots with error bars are data, and the shaded histogram are stacked MC samples of signal MC, $2(\pi^+\pi^-\pi^0)$ MC and $\omega\pi^+\pi^-$ MC. (b) Distribution of $M(\pi^+\pi^-\pi^0)$ in the η' signal region, where the (black) dots with error bars are data, and the shaded histogram are the stacked signal MC sample and non-η' events estimated by the η' sideband. (c) Fit to the $M(\gamma\pi^+\pi^-)$ distribution, where the (black) dots with error bars are data, the (blue) solid curve is the total fit result, the (green) dashed curve indicates the fitted background shape, and the (red) dash-dotted curve is the fitted signal shape. The vertical lines indicate the signal (red) and sideband regions (green). All the requirements mentioned above have been applied.

We performed an unbinned maximum likelihood fit to the $M(\gamma\pi^+\pi^-)$ spectrum and obtain the signal yields of the $e^+e^- \to \omega\eta'$. The signal is described by the signal MC-simulated shape convolved with a Gaussian function that describes the difference between data and MC simulation. The background function is parametrized by a second-order Chebychev function. The corresponding fit result for data taken at $\sqrt{s} = 2.125\,\text{GeV}$ is shown in figure 1(c). The same event selection criteria and fit procedure are applied for all data samples at different c.m. energies. The obtained signal yields are listed in table 2.

4 Born cross section and systematic uncertainty

The Born cross section for $e^+e^- \to \omega\eta'$ is calculated by

$$\sigma\left(\sqrt{s}\right) = \frac{N_{\text{sig}}}{\mathcal{L}\cdot\epsilon\cdot\mathcal{B}\cdot\frac{1}{|1-\Pi|^2}\cdot(1+\delta)}, \tag{4.1}$$

where N_{sig} is the number of signal events, $\mathcal{L}$ is the integrated luminosity, ϵ is the selection efficiency, $\mathcal{B}$ is the branching fraction $\mathcal{B} = \mathcal{B}_{\omega\to\pi^+\pi^-\pi^0}\cdot\mathcal{B}_{\eta'\to\gamma\pi^+\pi^-}\cdot\mathcal{B}_{\pi^0\to\gamma\gamma} = 26.0\%$, which

$\sqrt{s}$ (GeV)	N_{sig}	$N_{\mathrm{sig}}^{\mathrm{up}}$	$\mathcal{L}$ (pb^{-1})	$\epsilon \cdot (1+\delta)$	VP	σ (pb)	σ^{up}(pb)	Significance (σ)
2.0000	10.9 ± 5.6	<23.1	10.1	0.0988	1.037	$40.63 \pm 20.87 \pm 2.56$	<86.13	1.9
2.0500	10.5 ± 4.1	—	3.3	0.0986	1.038	$118.40 \pm 46.22 \pm 7.46$	—	3.6
2.1000	23.7 ± 6.8	—	12.2	0.0987	1.039	$72.43 \pm 20.78 \pm 4.56$	—	4.4
2.1250	273.7 ± 22.6	—	108.5	0.1000	1.039	$93.71 \pm 7.74 \pm 5.90$	—	15.6
2.1500	$8.8^{+4.3}_{-3.5}$	<16.6	2.8	0.1016	1.040	$113.00^{+55.22}_{-44.95} \pm 7.12$	<213.23	3.1
2.1750	13.8 ± 4.3	<22.5	10.6	0.1045	1.040	$46.02 \pm 14.34 \pm 2.90$	<75.05	3.4
2.2000	26.2 ± 8.0	—	13.7	0.1046	1.040	$67.40 \pm 20.58 \pm 4.25$	—	4.8
2.2324	$8.4^{+5.0}_{-4.3}$	<16.5	11.9	0.1046	1.041	$24.84^{+14.79}_{-12.72} \pm 1.56$	<48.80	2.2
2.3094	$0.4^{+4.1}_{-3.3}$	<8.4	21.1	0.1036	1.041	$0.67^{+6.91}_{-5.56} \pm 0.04$	<14.15	0.1
2.3864	$0.0^{+4.4}_{-3.6}$	<8.4	22.5	0.1063	1.041	$0.03^{+6.82}_{-5.58} \pm 0.00$	<13.02	0.0
2.3960	$3.6^{+6.6}_{-5.8}$	<16.5	66.9	0.1066	1.041	$1.85^{+3.40}_{-2.99} \pm 0.12$	<8.50	0.8
2.5000	$0.4^{+1.6}_{-0.0}$	<4.7	1.1	0.1127	1.041	$11.84^{+47.36}_{-79.91} \pm 0.85$	<139.11	0.1
2.6444	$9.5^{+4.5}_{-3.8}$	<16.4	33.7	0.1146	1.039	$9.08^{+4.30}_{-3.63} \pm 0.57$	<15.67	3.0
2.6464	$1.2^{+3.0}_{-2.3}$	<6.9	34.0	0.1151	1.039	$1.14^{+2.86}_{-2.19} \pm 0.07$	<6.57	0.5
2.7000	$0.0^{+0.6}_{-0.0}$	<3.9	1.0	0.1188	1.039	$0.00^{+18.63}_{-0.00} \pm 0.00$	<121.12	0.0
2.8000	$0.0^{+0.5}_{-0.0}$	<2.5	1.0	0.1185	1.037	$0.00^{+15.53}_{-0.00} \pm 0.00$	<77.64	0.0
2.9000	$1.5^{+3.8}_{-2.9}$	<8.7	105.3	0.1238	1.033	$0.43^{+1.10}_{-0.84} \pm 0.03$	<2.51	0.5
2.9500	$1.6^{+2.3}_{-1.6}$	<6.5	15.9	0.1208	1.029	$3.08^{+4.43}_{-3.08} \pm 0.19$	<12.51	1.6
2.9810	$3.4^{+2.9}_{-2.1}$	<8.5	16.1	0.1266	1.025	$6.30^{+5.38}_{-3.89} \pm 0.40$	<15.76	1.9
3.0000	$0.0^{+1.1}_{-2.1}$	<3.2	15.9	0.1270	1.021	$0.00^{+2.07}_{-3.95} \pm 0.00$	<6.02	0.0
3.0200	$0.3^{+1.5}_{-0.8}$	<3.2	17.3	0.1262	1.014	$0.52^{+2.60}_{-1.39} \pm 0.03$	<5.55	0.3
3.0800	$0.9^{+3.0}_{-2.1}$	<6.5	126.2	0.1298	0.915	$0.24^{+0.79}_{-0.55} \pm 0.02$	<1.70	0.4

Table 2. The Born cross sections for $e^+e^- \to \omega\eta'$. All definitions of symbols are the same as those in eq. (4.1). Upper limits are given at the 90% confidence level. For the Born cross section σ, the first uncertainty is statistical and the second is systematic. The VP column lists the vacuum polarization correction factor.

is taken from the PDG [1], $\frac{1}{|1-\Pi|^2}$ is the vacuum polarization factor (VP) [25], and $1+\delta$ is the ISR correction factor, which is obtained by a QED calculation [26] that takes the line shape of the Born cross section into account. Both ϵ and $1+\delta$ depend on the line shape of the cross sections and are determined via an iterative procedure [27, 28]. The ϵ and $1+\delta$ are calculated according to the fit curve and are taken as input for the next iteration. The procedure is repeated until the difference between the final measured Born cross sections and the last one less than 0.1%. The statistical significance of the signal for each energy point is estimated by considering the change of likelihood $\Delta(L)$ and the number of degrees of freedom in fits that include or do not include the signal function. For energy points where the significance of the signal is less than or close to 3σ, the upper limits for the number of signal events ($N_{\mathrm{sig}}^{\mathrm{up}}$) and the cross section (σ^{up}) are obtained using the profilelikelihood method [29]. The Born cross sections and upper limits at the 90% confidence level for all 22 energy points are summarized in table 2.

Various sources of systematic uncertainties concerning the measurement of the Born cross sections are investigated; these include the integrated luminosity, the charged track efficiency, the photon reconstruction efficiency, the PID efficiency, the kinematic fit, the requirement on

JHEP07(2024)093

$M(\pi^+\pi^-\pi^0)$, ISR and VP correction factors, input branching fractions, and the fit to the $M(\gamma\pi^+\pi^-)$ distribution. These sources are described as follows.

- The uncertainty associated with the integrated luminosity is 1%, which is estimated by using large angle Bhabha events in ref. [30].

- The uncertainties related to the tracking and PID efficiencies of charged pions are investigated using a control sample of $e^+e^- \to K^+K^-\pi^+\pi^-$ [28, 31]. The uncertainties on the tracking and PID efficiencies are estimated to be 1% per charged pion track.

- The uncertainty concerning the photon detection efficiency is studied with a control sample of $e^+e^- \to K^+K^-\pi^+\pi^-\pi^0$ [32]. The result shows that the difference in detection efficiency between data and MC simulation is 1% per photon.

- The uncertainties arising from the χ^2_{4C} requirement in the kinematic fit and the ω invariant mass requirement are evaluated from a control sample $J/\psi \to \omega\eta'$. The averaged difference between the data and MC simulation of $J/\psi \to \omega\eta'$ by using each requirement or not is taken as the systematic uncertainty.

- The uncertainty of the VP and ISR correction factors is obtained with the accuracy of the radiation function, which is about 0.5% [25], and has an additional contribution from the cross section line shape, which is estimated by varying the model parameters of the fit to the cross section. Considering correlations among the parameters, all parameters are randomly generated using a correlated multi-variable Gaussian function and the resulting parametrization of the line shape is used to recalculate $(1+\delta)\epsilon$ and the corresponding cross section. This procedure is repeated one thousand times and the standard deviation of the resulting cross section is considered. The systematic uncertainty associated with the VP and ISR correction factors is assigned as their quadratic sum [31].

- The uncertainty associated with the quoted branching fractions from the PDG [1] is 1.5%, including the effects of $\mathcal{B}_{\omega\to\pi^+\pi^-\pi^0} = (89.2 \pm 0.7)\%$, $\mathcal{B}_{\pi^0\to\gamma\gamma} = (98.823 \pm 0.034)\%$ and $\mathcal{B}_{\eta'\to\gamma\pi^+\pi^-} = (29.5 \pm 0.4)\%$.

- The uncertainty caused by the fit to the $M(\gamma\pi^+\pi^-)$ distribution includes the descriptions of the signal shape, background shape and fit range and is estimated by the control sample $J/\psi \to \omega\eta'$. The nominal MC-simulated shape convolved with a Gaussian function is replaced by a pure MC-simulated shape, and the difference is taken as the uncertainty. Replacing the nominal background shape by a first-order Chebychev function, the deviation from the nominal result is taken as the uncertainty. The fit range is varied by $\pm 10\,\mathrm{MeV}/c^2$ at both boundaries, and the largest difference is taken as the uncertainty. The uncertainties from these three sources are added in quadrature and taken as the total uncertainty from the $M(\gamma\pi^+\pi^-)$ fit.

Table 3 summarizes all the systematic uncertainties related to the Born cross section for each energy point, where the sources of the uncertainties tagged with '*' are assumed to be 100% correlated among c.m. energies. The total systematic uncertainty for each

$\sqrt{s}$ (GeV)	$\mathcal{L}^*$	Track*	Pho.*	PID*	Kin.*	ω Mass*	Rad.	Br*	Fit*	Sum
2.0000	1.0	4.0	3.0	4.0	0.2	0.9	0.6	1.5	2.4	7.1
2.0500	1.0	4.0	3.0	4.0	0.2	0.9	0.7	1.5	2.4	7.2
2.1000	1.0	4.0	3.0	4.0	0.2	0.9	1.5	1.5	2.4	7.3
2.1250	1.0	4.0	3.0	4.0	0.2	0.9	1.5	1.5	2.4	7.3
2.1500	1.0	4.0	3.0	4.0	0.2	0.9	1.1	1.5	2.4	7.2
2.1750	1.0	4.0	3.0	4.0	0.2	0.9	0.8	1.5	2.4	7.2
2.2000	1.0	4.0	3.0	4.0	0.2	0.9	0.7	1.5	2.4	7.2
2.2324	1.0	4.0	3.0	4.0	0.2	0.9	0.6	1.5	2.4	7.2
2.3094	1.0	4.0	3.0	4.0	0.2	0.9	0.6	1.5	2.4	7.2
2.3864	1.0	4.0	3.0	4.0	0.2	0.9	0.6	1.5	2.4	7.2
2.3960	1.0	4.0	3.0	4.0	0.2	0.9	0.6	1.5	2.4	7.2
2.5000	1.0	4.0	3.0	4.0	0.2	0.9	0.6	1.5	2.4	7.2
2.6444	1.0	4.0	3.0	4.0	0.2	0.9	0.5	1.5	2.4	7.2
2.6464	1.0	4.0	3.0	4.0	0.2	0.9	0.6	1.5	2.4	7.2
2.7000	1.0	4.0	3.0	4.0	0.2	0.9	0.6	1.5	2.4	7.2
2.8000	1.0	4.0	3.0	4.0	0.2	0.9	0.5	1.5	2.4	7.2
2.9000	1.0	4.0	3.0	4.0	0.2	0.9	0.5	1.5	2.4	7.2
2.9500	1.0	4.0	3.0	4.0	0.2	0.9	0.5	1.5	2.4	7.2
2.9810	1.0	4.0	3.0	4.0	0.2	0.9	0.5	1.5	2.4	7.2
3.0000	1.0	4.0	3.0	4.0	0.2	0.9	0.5	1.5	2.4	7.2
3.0200	1.0	4.0	3.0	4.0	0.2	0.9	0.5	1.5	2.4	7.2
3.0800	1.0	4.0	3.0	4.0	0.2	0.9	0.5	1.5	2.4	7.2

Table 3. Systematic uncertainties (in %) in the Born cross section of $e^+e^- \to \omega\eta'$ at each energy point. These represent the uncertainties in the estimated effects of the integrated luminosity ($\mathcal{L}$), tracking efficiency (Track), photon reconstruction efficiency (Pho.), PID efficiency (PID), kinematic fit (Kin.), ω mass window (ω Mass), VP and ISR correction factor (Rad.), branching fraction (Br) and $M(\gamma\pi^+\pi^-)$ fit (Fit). The total uncertainty (Sum) is obtained by summing the individual contributions in quadrature.

energy point is calculated as the quadratic sum of the individual uncertainties, assuming they are independent.

5 Fit to the line shape

Figure 2 shows the measured Born cross sections, where a clear structure is visible around 2.2 GeV. We perform a χ^2 fit to extract resonance parameters, incorporating the correlated and uncorrelated uncertainties among different energy points. The fit probability density function is a coherent sum of a continuum component f_1 and a resonant component f_2. The cross section is modeled as

$$\sigma = \frac{12\pi}{s^{3/2}}|f_1 + e^{i\phi} f_2|^2 PS\left(\sqrt{s}\right), \tag{5.1}$$

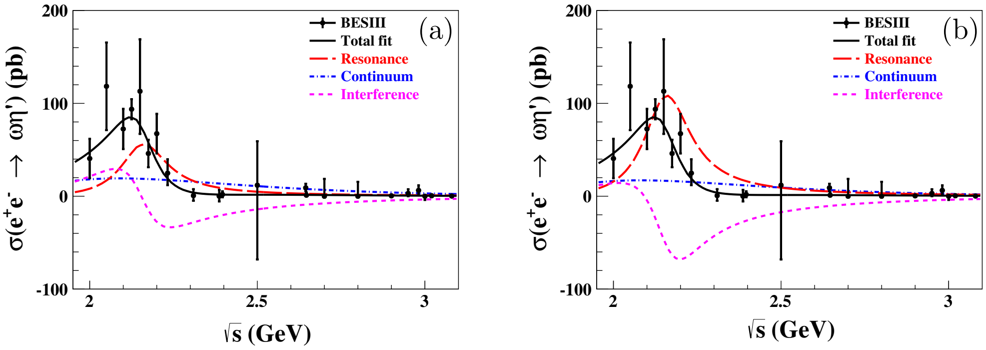

Figure 2. The Born cross section and fit curves, (a) and (b), corresponding to the two solutions shown in table 4. Dots with error bars are BESIII data, where errors include both statistical and systematic uncertainties. The solid (black) curves represent the total fit result, the dashed (red) curves are for the intermediate state and the dash-dotted (blue) curves are for the continuum component, and the intensive dash-dotted (magenta) curves are for the interference between the resonance and continuum components.

where ϕ is the relative phase between these two components, and $PS(\sqrt{s})$ is the phase-space factor [10] given by $PS(\sqrt{s}) = q^3$, where q is the ω momentum in the e^+e^- c.m. frame calculated for the mass value $M_\omega = 0.78265\,\mathrm{GeV}/c^2$ [1]. The contribution from lower-mass vector states is considered in the description of f_1 as

$$f_1 = C_0 \cdot e^{-p_0\left(\sqrt{s}-M_{\mathrm{th}}\right)}, \tag{5.2}$$

where C_0 and p_0 are free parameters, and $M_{\mathrm{th}} = 1.7404\,\mathrm{GeV}/c^2$ is the mass threshold for $\omega\eta'$ production [1, 33]. The resonant amplitude f_2 is described by a Breit-Wigner (BW) function:

$$f_2 = \sqrt{\frac{\Gamma_R^{e^+e^-} \cdot B_R^{\omega\eta'}}{PS(m_R)}}\,\frac{m_R^{3/2}\sqrt{\Gamma_R}}{s - m_R^2 + i\sqrt{s}\Gamma_R}, \tag{5.3}$$

where m_R and Γ_R are the mass and width of the resonant structure, $\Gamma_R^{e^+e^-}$ is its partial width to e^+e^-, and B_R is the branching fraction of $R \to \omega\eta'$.

In total, there are six free parameters in the fit: $\phi, C_0, p_0, m_R, \Gamma_R$ and the product of $\Gamma_R^{e^+e^-} B_R$. The fit results are shown in figure 2, and resonance parameters are listed in table 4. The fit has two solutions with identical mass and width for the resonance. The two solutions for the phase ϕ and $\Gamma_R^{e^+e^-} B_R$ are consistent with each other considering their uncertainties. The fit quality is $\chi^2/\mathrm{ndf} = 13.5/16$, where ndf is the number of degrees of freedom. The mass and width of the resonance are $M_R = (2153 \pm 30)$ MeV/c^2 and $\Gamma_R = (167 \pm 77)$ MeV, respectively, where the uncertainties are statistical only. The significance of the resonance is determined to be 9.6σ by comparing the change of the χ^2 in fits with and without the resonance and considering the change in ndf. The uncertainties (statistical and systematic) of the measured Born cross sections have been considered when fitting the line shape, extracting the resonance parameters and estimating the significance of the resonance.

The systematic uncertainties of the resonant parameters are due to the c.m. energy from BEPCII and the formula used in the fit procedure. The uncertainty of the c.m.

Parameter	Solution 1	Solution 2
M_R (MeV/c^2)	$2153 \pm 30(\text{stat.}) \pm 31(\text{syst.})$	
Γ_R (MeV)	$167 \pm 77(\text{stat.}) \pm 7(\text{syst.})$	
ϕ (rad)	$3.78 \pm 0.24(\text{stat.}) \pm 0.12(\text{syst.})$	$3.16 \pm 0.4(\text{stat.}) \pm 0.2(\text{syst.})$
$\Gamma_R^{e^+e^-}\mathcal{B}_{\mathcal{R}}^{\omega\eta'}$ (eV)	$5.72 \pm 1.68(\text{stat.}) \pm 1.5(\text{syst.})$	$2.99 \pm 1.68(\text{stat.}) \pm 1.2(\text{syst.})$
Significance	9.6σ	

Table 4. The obtained resonance parameters.

energy calibration is estimated as 0.1%. It is ignored in the determination of the resonance parameters [30]. To evaluate the systematic uncertainty associated with the fit formula, the continuum term $C_0 \cdot e^{-p_0(\sqrt{s}-M_{\text{th}})}$ is replaced with an exponential function of the form c_1/s^{c_2}, where c_1 and c_2 are free parameters and the width Γ_R is replaced with an energy-dependent width of the form $\Gamma_R(\sqrt{s}) = \Gamma_R \cdot \frac{PS(\sqrt{s})}{PS(M_R)}$ [33]. The deviation of the obtained parameters from the nominal results are taken as the systematic uncertainties. The resonance parameters, which have been considered systematically, are listed in table 4.

6 Summary

In summary, we measured the Born cross sections of the process $e^+e^- \to \omega\eta'$ at center-of-mass energies from 2.000 to 3.080 GeV using 22 data samples corresponding to a total integrated luminosity of 650 pb^{-1} collected by the BESIII detector. By analyzing the energy dependence of the cross sections, a structure is observed with a statistical significance of 9.6σ with mass $M_R = (2153 \pm 30 \pm 31)$ MeV/c^2 and width $\Gamma_R = (167 \pm 77 \pm 7)$ MeV, where the first and second uncertainties are statistical and systematic, respectively.

Compared to the resonance parameters for structures around 2.2 GeV obtained from the previous BESIII measurements via $e^+e^- \to \omega\eta$ [10], $e^+e^- \to \omega\pi^0\pi^0$ [11] and $e^+e^- \to \omega\pi^+\pi^-$ [12], $M_1 = 2176 \pm 24$ MeV/c^2, $\Gamma_1 = 89 \pm 50$ MeV and $M_2 = 2232 \pm 19$ MeV/c^2, $\Gamma_2 = 93 \pm 53$ MeV, respectively, the parameters obtained in this work are in agreement with them within 3σ.

Supposing the resonances around 2.2 GeV observed in $R \to \omega\eta$ and $R \to \omega\eta'$ are the same, and R only contains $u\bar{u}$ and $d\bar{d}$ quarks, the ratio between branching fractions of $R \to \omega\eta$ and $R \to \omega\eta'$ can be written as

$$\frac{B_R^{\omega\eta'}}{B_R^{\omega\eta}} = \left|\frac{\cos(\Theta_0 - \Theta)}{\sin(\Theta_0 - \Theta)}\right|^2 \frac{\Omega_{\eta'}}{\Omega_\eta}, \tag{6.1}$$

where $\Theta_0 = 35.3^\circ$ is the ideal mixing angle between pure $s\bar{s}$ and $u\bar{u} - d\bar{d}$, and $\Omega_{\eta'}(\Omega_\eta)$ is the phase-space factor including the P-wave effect in decay [34, 35]. Based on the suggested mixing angle $\Theta = -14.1 \pm 2.8^\circ$ calculated by lattice QCD [1, 36], the ratio between $\Gamma_R^{e^+e^-}\mathcal{B}_{\mathcal{R}}^{\omega\eta'}$ and $\Gamma_R^{e^+e^-}\mathcal{B}_{\mathcal{R}}^{\omega\eta}$ is 0.34 ± 0.07. Combining our results with the previous BESIII measurements of the $e^+e^- \to \omega\eta$ process [10], and taking into account the mutiple solutions for the resonance parameters, these ratios are measured to be $13.30 \pm 6.06 \pm 3.61$, $2.39 \pm 1.63 \pm 1.01$, $4.58 \pm 2.21 \pm 1.34$ and $6.95 \pm 4.60 \pm 2.83$, where the first and second uncertainties are statistical and systematic, respectively. All of them are greater than 0.34 ± 0.07 based on the $\eta - \eta'$ mixing angle given by lattice QCD. Future experimental and theoretical studies will be helpful to improve the knowledge of excited ω states around 2.2 GeV.

Acknowledgments

The BESIII Collaboration thanks the staff of BEPCII, the IHEP computing center and the supercomputing center of USTC for their strong support. This work is supported in part by National Key R&D Program of China under Contracts Nos. 2020YFA0406400, 2020YFA0406300; National Natural Science Foundation of China (NSFC) under Contracts Nos. 11635010, 11735014, 11835012, 11935015, 11935016, 11935018, 11961141012, 12022510, 12025502, 12035009, 12035013, 12192260, 12192261, 12192262, 12192263, 12192264, 12192265, 12275320, 11625523, 11705192, 11950410506, 12061131003, 12105276, 12122509, 12205255; the Chinese Academy of Sciences (CAS) Large-Scale Scientific Facility Program; the CAS Center for Excellence in Particle Physics (CCEPP); Joint Large-Scale Scientific Facility Funds of the NSFC and CAS under Contracts Nos. U1832207, U1732263, U1832103, U2032111; CAS Key Research Program of Frontier Sciences under Contracts Nos. QYZDJ-SSW-SLH003, QYZDJ-SSW-SLH040; 100 Talents Program of CAS; The Institute of Nuclear and Particle Physics (INPAC) and Shanghai Key Laboratory for Particle Physics and Cosmology; ERC under Contract No. 758462; European Union's Horizon 2020 research and innovation programme under Marie Sklodowska-Curie grant agreement under Contract No. 894790; German Research Foundation DFG under Contracts Nos. 443159800, 455635585, Collaborative Research Center CRC 1044, FOR5327, GRK 2149; Istituto Nazionale di Fisica Nucleare, Italy; Ministry of Development of Turkey under Contract No. DPT2006K-120470; National Research Foundation of Korea under Contract No. NRF-2022R1A2C1092335; National Science and Technology fund; National Science Research and Innovation Fund (NSRF) via the Program Management Unit for Human Resources & Institutional Development, Research and Innovation under Contract No. B16F640076; Polish National Science Centre under Contract No. 2019/35/O/ST2/02907; The Royal Society, U.K. under Contracts Nos. DH140054, DH160214; The Swedish Research Council; U.S. Department of Energy under Contract No. DE-FG02-05ER41374.

References

[1] Particle Data Group collaboration, *Review of Particle Physics*, *PTEP* **2022** (2022) 083C01 [inSPIRE].

[2] A.V. Anisovich et al., $I = 0, C = -1$ *mesons from 1940 to 2410 MeV*, *Phys. Lett. B* **542** (2002) 19 [arXiv:1109.5817] [inSPIRE].

[3] D.V. Bugg, *Partial wave analysis of* $\bar{p}p \to \bar{\Lambda}\Lambda$, *Eur. Phys. J. C* **36** (2004) 161 [hep-ph/0406292] [inSPIRE].

[4] Omega Photon collaboration, *Photon diffractive dissociation to $\rho\rho\pi$ and $\rho\pi\pi\pi$ states*, *Z. Phys. C* **38** (1988) 535 [INSPIRE].

[5] C.-Q. Pang et al., *Study of the ω meson family and newly observed ω-like state $X(2240)$*, *Phys. Rev. D* **101** (2020) 074022 [arXiv:1910.12408] [INSPIRE].

[6] J.-C. Feng, X.-W. Kang, Q.-F. Lü and F.-S. Zhang, *Possible assignment of excited light $^3S_1$ vector mesons*, *Phys. Rev. D* **104** (2021) 054027 [arXiv:2104.01339] [INSPIRE].

[7] Y.-R. Wang et al., *Study of the ω and ω_3, ρ and ρ_3, and the newly observed ω-like state X(2220)*, *Phys. Rev. D* **106** (2022) 114024 [arXiv:2208.10329] [INSPIRE].

[8] BaBar collaboration, *The $e^+e^- \to 2(\pi^+\pi^-)\pi^0, 2(\pi^+\pi^-)\eta, K^+K^-\pi^+\pi^-\pi^0$ and $K^+K^-\pi^+\pi^-\eta$ Cross Sections Measured with Initial-State Radiation*, *Phys. Rev. D* **76** (2007) 092005 [*Erratum ibid.* **77** (2008) 119902] [arXiv:0708.2461] [INSPIRE].

[9] BaBar collaboration, *Resonances in e^+e^- annihilation near 2.2 GeV*, *Phys. Rev. D* **101** (2020) 012011 [arXiv:1912.04512] [INSPIRE].

[10] BESIII collaboration, *Observation of a resonant structure in $e^+e^- \to \omega\eta$ and another in $e^+e^- \to \omega\pi^0$ at center-of-mass energies between 2.00 and 3.08 GeV*, *Phys. Lett. B* **813** (2021) 136059 [arXiv:2009.08099] [INSPIRE].

[11] BESIII collaboration, *Measurement of the $e^+e^- \to \omega\pi^0\pi^0$ cross section at center-of-mass energies from 2.0 to 3.08 GeV*, *Phys. Rev. D* **105** (2022) 032005 [arXiv:2112.15076] [INSPIRE].

[12] BESIII collaboration, *Measurement of $e^+e^- \to \omega\pi^+\pi^-$ cross section at $\sqrt{s} = 2.000$ to 3.080 GeV*, *JHEP* **01** (2023) 111 [*Erratum ibid.* **03** (2023) 093] [arXiv:2208.04507] [INSPIRE].

[13] Q.-S. Zhou, J.-Z. Wang and X. Liu, *Role of the $\omega(4S)$ and $\omega(3D)$ states in mediating the $e^+e^- \to \omega\eta$ and $\omega\pi^0\pi^0$ processes*, *Phys. Rev. D* **106** (2022) 034010 [arXiv:2207.00276] [INSPIRE].

[14] BESIII collaboration, *Design and construction of the BESIII detector*, *Nucl. Instrum. Meth. A* **614** (2010) 345 [arXiv:0911.4960] [INSPIRE].

[15] C. Yu et al., *BEPCII Performance and Beam Dynamics Studies on Luminosity*, in the proceedings of the *7th International Particle Accelerator Conference*, Busan, South Korea, May 08–13 (2016) [DOI:10.18429/JACoW-IPAC2016-TUYA01] [INSPIRE].

[16] BESIII collaboration, *Future Physics Programme of BESIII*, *Chin. Phys. C* **44** (2020) 040001 [arXiv:1912.05983] [INSPIRE].

[17] GEANT4 collaboration, *GEANT4 — a simulation toolkit*, *Nucl. Instrum. Meth. A* **506** (2003) 250 [INSPIRE].

[18] K.-X. Huang et al., *Method for detector description transformation to Unity and application in BESIII*, *Nucl. Sci. Tech.* **33** (2022) 142 [arXiv:2206.10117] [INSPIRE].

[19] R.-G. Ping, *An exclusive event generator for e^+e^- scan experiments*, *Chin. Phys. C* **38** (2014) 083001 [arXiv:1309.3932] [INSPIRE].

[20] BESIII collaboration, *Precision Study of $\eta' \to \gamma\pi^+\pi^-$ Decay Dynamics*, *Phys. Rev. Lett.* **120** (2018) 242003 [arXiv:1712.01525] [INSPIRE].

[21] BESIII collaboration, *Dalitz Plot Analysis of the Decay $\omega \to \pi^+\pi^-\pi^0$*, *Phys. Rev. D* **98** (2018) 112007 [arXiv:1811.03817] [INSPIRE].

[22] B. Andersson and H.-M. Hu, *Few body states in Lund string fragmentation model*, hep-ph/9910285 [INSPIRE].

[23] H. Czyż, P. Kisza and S. Tracz, *Modeling interactions of photons with pseudoscalar and vector mesons*, Phys. Rev. D **97** (2018) 016006 [`arXiv:1711.00820`] [INSPIRE].

[24] BABAR collaboration, *The $e^+e^- \to 3(\pi^+\pi^-), 2(\pi^+\pi^-\pi^0)$ and $K^+K^-2(\pi^+\pi^-)$ cross sections at center-of-mass energies from production threshold to 4.5-GeV measured with initial-state radiation*, Phys. Rev. D **73** (2006) 052003 [`hep-ex/0602006`] [INSPIRE].

[25] WORKING GROUP ON RADIATIVE CORRECTIONS and MONTE CARLO GENERATORS FOR LOW ENERGIES collaborations, *Quest for precision in hadronic cross sections at low energy: Monte Carlo tools vs. experimental data*, Eur. Phys. J. C **66** (2010) 585 [`arXiv:0912.0749`] [INSPIRE].

[26] E.A. Kuraev and V.S. Fadin, *On Radiative Corrections to e^+e^- Single Photon Annihilation at High-Energy*, Sov. J. Nucl. Phys. **41** (1985) 466 [INSPIRE].

[27] W. Sun et al., *An iterative weighting method to apply ISR correction to e^+e^- hadronic cross-section measurements*, Front. Phys. (Beijing) **16** (2021) 64501 [`arXiv:2011.07889`] [INSPIRE].

[28] BESIII collaboration, *Cross section measurement of $e^+e^- \to K_S^0K_L^0$ at $\sqrt{s} = 2.00 - 3.08$ GeV*, Phys. Rev. D **104** (2021) 092014 [`arXiv:2105.13597`] [INSPIRE].

[29] J. Lundberg, J. Conrad, W. Rolke and A. Lopez, *Limits, discovery and cut optimization for a Poisson process with uncertainty in background and signal efficiency: TRolke 2.0*, Comput. Phys. Commun. **181** (2010) 683 [`arXiv:0907.3450`] [INSPIRE].

[30] BESIII collaboration, *Luminosity measurements for the R scan experiment at BESIII*, Chin. Phys. C **41** (2017) 063001 [`arXiv:1702.04977`] [INSPIRE].

[31] BESIII collaboration, *Measurement of $e^+e^- \to K^+K^-$ cross section at $\sqrt{s} = 2.00 - 3.08$ GeV*, Phys. Rev. D **99** (2019) 032001 [`arXiv:1811.08742`] [INSPIRE].

[32] W.-L. Yuan et al., *Study of tracking efficiency and its systematic uncertainty from $J/\psi \to p\bar{p}\pi^+\pi^-$ at BESIII*, Chin. Phys. C **40** (2016) 026201 [`arXiv:1507.03453`] [INSPIRE].

[33] BESIII collaboration, *Measurement of $e^+e^- \to K^+K^-\pi^0$ cross section and observation of a resonant structure*, JHEP **07** (2022) 045 [`arXiv:2202.06447`] [INSPIRE].

[34] K. Zhu, *Selecting the physical solution via η-η' mixing*, Phys. Rev. D **105** (2022) L031506 [`arXiv:2109.01367`] [INSPIRE].

[35] R. Sinha and S. Okubo, *Analysis of $\psi/J \to p\bar{p}\pi^0$, η, and η' Decays*, Phys. Rev. D **30** (1984) 2333 [INSPIRE].

[36] N.H. Christ et al., *The η and η' mesons from Lattice QCD*, Phys. Rev. Lett. **105** (2010) 241601 [`arXiv:1002.2999`] [INSPIRE].

JHEP07(2024)093

The BESIII collaboration

M. Ablikim[1], M.N. Achasov[5,b], P. Adlarson[74], X.C. Ai[80], R. Aliberti[35], A. Amoroso[73A,73C], M.R. An[39], Q. An[70,57], Y. Bai[56], O. Bakina[36], I. Balossino[29A], Y. Ban[46,g], V. Batozskaya[1,44], K. Begzsuren[32], N. Berger[35], M. Berlowski[44], M. Bertani[28A], D. Bettoni[29A], F. Bianchi[73A,73C], E. Bianco[73A,73C], A. Bortone[73A,73C], I. Boyko[36], R.A. Briere[6], A. Brueggemann[67], H. Cai[75], X. Cai[1,57], A. Calcaterra[28A], G.F. Cao[1,62], N. Cao[1,62], S.A. Cetin[61A], J.F. Chang[1,57], T.T. Chang[76], W.L. Chang[1,62], G.R. Che[43], G. Chelkov[36,a], C. Chen[43], Chao Chen[54], G. Chen[1], H.S. Chen[1,62], M.L. Chen[1,57,62], S.J. Chen[42], S.M. Chen[60], T. Chen[1,62], X.R. Chen[31,62], X.T. Chen[1,62], Y.B. Chen[1,57], Y.Q. Chen[34], Z.J. Chen[25,h], W.S. Cheng[73C], S.K. Choi[11], X. Chu[43], G. Cibinetto[29A], S.C. Coen[4], F. Cossio[73C], J.J. Cui[49], H.L. Dai[1,57], J.P. Dai[78], A. Dbeyssi[18], R. E. de Boer[4], D. Dedovich[36], Z.Y. Deng[1], A. Denig[35], I. Denysenko[36], M. Destefanis[73A,73C], F. De Mori[73A,73C], B. Ding[65,1], X.X. Ding[46,g], Y. Ding[40], Y. Ding[34], J. Dong[1,57], L.Y. Dong[1,62], M.Y. Dong[1,57,62], X. Dong[75], M.C. Du[1], S.X. Du[80], Z.H. Duan[42], P. Egorov[36,a], Y.H.Y. Fan[45], Y.L. Fan[75], J. Fang[1,57], S.S. Fang[1,62], W.X. Fang[1], Y. Fang[1], R. Farinelli[29A], L. Fava[73B,73C], F. Feldbauer[4], G. Felici[28A], C.Q. Feng[70,57], J.H. Feng[58], K Fischer[68], M. Fritsch[4], C. Fritzsch[67], C.D. Fu[1], J.L. Fu[62], Y.W. Fu[1], H. Gao[62], Y.N. Gao[46,g], Yang Gao[70,57], S. Garbolino[73C], I. Garzia[29A,29B], P.T. Ge[75], Z.W. Ge[42], C. Geng[58], E.M. Gersabeck[66], A Gilman[68], K. Goetzen[14], L. Gong[40], W.X. Gong[1,57], W. Gradl[35], S. Gramigna[29A,29B], M. Greco[73A,73C], M.H. Gu[1,57], C. Y Guan[1,62], Z.L. Guan[22], A.Q. Guo[31,62], L.B. Guo[41], M.J. Guo[49], R.P. Guo[48], Y.P. Guo[13,f], A. Guskov[36,a], T.T. Han[49], W.Y. Han[39], X.Q. Hao[19], F.A. Harris[64], K.K. He[54], K.L. He[1,62], F.H.H. Heinsius[4], C.H. Heinz[35], Y.K. Heng[1,57,62], C. Herold[59], T. Holtmann[4], P.C. Hong[13,f], G.Y. Hou[1,62], X.T. Hou[1,62], Y.R. Hou[62], Z.L. Hou[1], H.M. Hu[1,62], J.F. Hu[55,i], T. Hu[1,57,62], Y. Hu[1], G.S. Huang[70,57], K.X. Huang[58], L.Q. Huang[31,62], X.T. Huang[49], Y.P. Huang[1], T. Hussain[72], N Hüsken[27,35], W. Imoehl[27], J. Jackson[27], S. Jaeger[4], S. Janchiv[32], J.H. Jeong[11], Q. Ji[1], Q.P. Ji[19], X.B. Ji[1,62], X.L. Ji[1,57], Y.Y. Ji[49], X.Q. Jia[49], Z.K. Jia[70,57], H.J. Jiang[75], P.C. Jiang[46,g], S.S. Jiang[39], T.J. Jiang[16], X.S. Jiang[1,57,62], Y. Jiang[62], J.B. Jiao[49], Z. Jiao[23], S. Jin[42], Y. Jin[65], M.Q. Jing[1,62], T. Johansson[74], X. Kui[1], S. Kabana[33], N. Kalantar-Nayestanaki[63], X.L. Kang[10], X.S. Kang[40], R. Kappert[63], M. Kavatsyuk[63], B.C. Ke[80], A. Khoukaz[67], R. Kiuchi[1], R. Kliemt[14], O.B. Kolcu[61A], B. Kopf[4], M. Kuessner[4], A. Kupsc[44,74], W. Kühn[37], J.J. Lane[66], P. Larin[18], A. Lavania[26], L. Lavezzi[73A,73C], T.T. Lei[70,k], Z.H. Lei[70,57], H. Leithoff[35], M. Lellmann[35], T. Lenz[35], C. Li[47], C. Li[43], C.H. Li[39], Cheng Li[70,57], D.M. Li[80], F. Li[1,57], G. Li[1], H. Li[70,57], H.B. Li[1,62], H.J. Li[19], H.N. Li[55,i], Hui Li[43], J.R. Li[60], J.S. Li[58], J.W. Li[49], K.L. Li[19], Ke Li[1], L. J Li[1,62], L.K. Li[1], Lei Li[3], M.H. Li[43], P.R. Li[38,j,k], Q.X. Li[49], S.X. Li[13], T. Li[49], W.D. Li[1,62], W.G. Li[1], X.H. Li[70,57], X.L. Li[49], Xiaoyu Li[1,62], Y.G. Li[46,g], Z.J. Li[58], C. Liang[42], H. Liang[1,62], H. Liang[70,57], H. Liang[34], Y.F. Liang[53], Y.T. Liang[31,62], G.R. Liao[15], L.Z. Liao[49], Y.P. Liao[1,62], J. Libby[26], A. Limphirat[59], D.X. Lin[31,62], T. Lin[1], B.J. Liu[1], B.X. Liu[75], C. Liu[34], C.X. Liu[1], F.H. Liu[52], Fang Liu[1], Feng Liu[7], G.M. Liu[55,i], H. Liu[38,j,k], H.M. Liu[1,62], Huanhuan Liu[1], Huihui Liu[21], J.B. Liu[70,57], J.L. Liu[71], J.Y. Liu[1,62], K. Liu[1], K.Y. Liu[40], Ke Liu[22], L. Liu[70,57], L.C. Liu[43], Lu Liu[43], M.H. Liu[13,f], P.L. Liu[1], Q. Liu[62], S.B. Liu[70,57], T. Liu[13,f], W.K. Liu[43], W.M. Liu[70,57], X. Liu[38,j,k], Y. Liu[38,j,k], Y. Liu[80], Y.B. Liu[43], Z.A. Liu[1,57,62], Z.Q. Liu[49], X.C. Lou[1,57,62], F.X. Lu[58], H.J. Lu[23], J.G. Lu[1,57], X.L. Lu[1], Y. Lu[8], Y.P. Lu[1,57], Z.H. Lu[1,62], C.L. Luo[41], M.X. Luo[79], T. Luo[13,f], X.L. Luo[1,57], X.R. Lyu[62], Y.F. Lyu[43], F.C. Ma[40], H.L. Ma[1], J.L. Ma[1,62], L.L. Ma[49], M.M. Ma[1,62], Q.M. Ma[1], R.Q. Ma[1,62], R.T. Ma[62], X.Y. Ma[1,57], Y. Ma[46,g], Y.M. Ma[31], F.E. Maas[18], M. Maggiora[73A,73C], S. Malde[68], Q.A. Malik[72], A. Mangoni[28B], Y.J. Mao[46,g], Z.P. Mao[1], S. Marcello[73A,73C], Z.X. Meng[65], J.G. Messchendorp[14,63], G. Mezzadri[29A], H. Miao[1,62], T.J. Min[42], R.E. Mitchell[27], X.H. Mo[1,57,62], N. Yu. Muchnoi[5,b], J. Muskalla[35], Y. Nefedov[36], F. Nerling[18,d], I.B. Nikolaev[5,b], Z. Ning[1,57], S. Nisar[12,l], Y. Niu [49], S.L. Olsen[62], Q. Ouyang[1,57,62], S. Pacetti[28B,28C], X. Pan[54], Y. Pan[56], A. Pathak[34], P. Patteri[28A], Y.P. Pei[70,57], M. Pelizaeus[4], H.P. Peng[70,57], K. Peters[14,d], J.L. Ping[41], R.G. Ping[1,62], S. Plura[35], S. Pogodin[36], V. Prasad[33], F.Z. Qi[1], H. Qi[70,57], H.R. Qi[60], M. Qi[42], T.Y. Qi[13,f], S. Qian[1,57], W.B. Qian[62], C.F. Qiao[62], J.J. Qin[71], L.Q. Qin[15], X.P. Qin[13,f], X.S. Qin[49], Z.H. Qin[1,57], J.F. Qiu[1], S.Q. Qu[60], C.F. Redmer[35], K.J. Ren[39], A. Rivetti[73C], V. Rodin[63], M. Rolo[73C], G. Rong[1,62], Ch. Rosner[18], S.N. Ruan[43], N. Salone[44], A. Sarantsev[36,c], Y. Schelhaas[35], K. Schoenning[74], M. Scodeggio[29A,29B], K.Y. Shan[13,f], W. Shan[24], X.Y. Shan[70,57], J.F. Shangguan[54], L.G. Shao[1,62], M. Shao[70,57], C.P. Shen[13,f], H.F. Shen[1,62], W.H. Shen[62], X.Y. Shen[1,62], B.A. Shi[62], H.C. Shi[70,57], J.L. Shi[13], J.Y. Shi[1], Q.Q. Shi[54], R.S. Shi[1,62], X. Shi[1,57], J.J. Song[19], T.Z. Song[58], W.M. Song[34,1], Y. J. Song[13], Y.X. Song[46,g], S. Sosio[73A,73C], S. Spataro[73A,73C], F. Stieler[35], Y.J. Su[62], G.B. Sun[75], G.X. Sun[1], H. Sun[62], H.K. Sun[1], J.F. Sun[19], K. Sun[60], L. Sun[75], S.S. Sun[1,62], T. Sun[1,62], W.Y. Sun[34], Y. Sun[10], Y.J. Sun[70,57], Y.Z. Sun[1], Z.T. Sun[49], Y.X. Tan[70,57], C.J. Tang[53], G.Y. Tang[1], J. Tang[58], Y.A. Tang[75], L. Y Tao[71], Q.T. Tao[25,h], M. Tat[68], J.X. Teng[70,57], V. Thoren[74], W.H. Tian[58], W.H. Tian[51], Y. Tian[31,62], Z.F. Tian[75], I. Uman[61B], S.J. Wang[49], B. Wang[1], B.L. Wang[62], Bo Wang[70,57], C.W. Wang[42], D.Y. Wang[46,g], F. Wang[71], H.J. Wang[38,j,k], H.P. Wang[1,62], J.P. Wang [49], K. Wang[1,57], L.L. Wang[1], M. Wang[49], Meng Wang[1,62], S. Wang[13,f], S. Wang[38,j,k], T. Wang[13,f], T.J. Wang[43], W. Wang[58], W. Wang[71], W.P. Wang[70,57], X. Wang[46,g], X.F. Wang[38,j,k], X.J. Wang[39], X.L. Wang[13,f], Y. Wang[60], Y.D. Wang[45], Y.F. Wang[1,57,62], Y.H. Wang[47], Y.N. Wang[45], Y.Q. Wang[1], Yaqian Wang[17,1], Yi Wang[60], Z. Wang[1,57], Z.L. Wang[71], Z.Y. Wang[1,62], Ziyi Wang[62], D. Wei[69], D.H. Wei[15], F. Weidner[67], S.P. Wen[1], C.W. Wenzel[4], U. Wiedner[4], G. Wilkinson[68], M. Wolke[74], L. Wollenberg[4], C. Wu[39], J.F. Wu[1,62], L.H. Wu[1], L.J. Wu[1,62], X. Wu[13,f], X.H. Wu[34], Y. Wu[70,57], Y.J. Wu[31], Z. Wu[1,57], L. Xia[70,57], X.M. Xian[39], T. Xiang[46,g], D. Xiao[38,j,k], G.Y. Xiao[42], S.Y. Xiao[1], Y.L. Xiao[13,f], Z.J. Xiao[41], C. Xie[42], X.H. Xie[46,g], Y. Xie[49], Y.G. Xie[1,57], Y.H. Xie[7], Z.P. Xie[70,57], T.Y. Xing[1,62], C.F. Xu[1,62], C.J. Xu[58], G.F. Xu[1], H.Y. Xu[65], Q.J. Xu[16], Q.N. Xu[30], W. Xu[1,62], W.L. Xu[65], X.P. Xu[54], Y.C. Xu[77], Z.P. Xu[42], Z.S. Xu[62], F. Yan[13,f], L. Yan[13,f], W.B. Yan[70,57], W.C. Yan[80], X.Q. Yan[1], H.J. Yang[50,e], H.L. Yang[34], H.X. Yang[1], Tao Yang[1], Y. Yang[13,f], Y.F. Yang[43], Y.X. Yang[1,62], Yifan Yang[1,62], Z.W. Yang[38,j,k], Z.P. Yao[49], M. Ye[1,57], M.H. Ye[9], J.H. Yin[1], Z.Y. You[58], B.X. Yu[1,57,62], C.X. Yu[43], G. Yu[1,62], J.S. Yu[25,h], T. Yu[71], X.D. Yu[46,g], C.Z. Yuan[1,62], L. Yuan[2], S.C. Yuan[1], X.Q. Yuan[1], Y. Yuan[1,62], Z.Y. Yuan[58], C.X. Yue[39], A.A. Zafar[72], F.R. Zeng[49], X. Zeng[13,f], Y. Zeng[25,h], Y.J. Zeng[1,62], X.Y. Zhai[34], Y.C. Zhai[49], Y.H. Zhan[58], A.Q. Zhang[1,62], B.L. Zhang[1,62], B.X. Zhang[1], D.H. Zhang[43], G.Y. Zhang[19], H. Zhang[70], H.H. Zhang[58], H.H. Zhang[34], H.Q. Zhang[1,57,62], H.Y. Zhang[1,57], J. Zhang[80], J.J. Zhang[51], J.L. Zhang[20], J.Q. Zhang[41], J.W. Zhang[1,57,62], J.X. Zhang[38,j,k], J.Y. Zhang[1], J.Z. Zhang[1,62], Jianyu Zhang[62], Jiawei Zhang[1,62], L.M. Zhang[60], L.Q. Zhang[58], Lei Zhang[42], P. Zhang[1,62], Q.Y. Zhang[39,80], Shuihan Zhang[1,62], Shulei Zhang[25,h], X.D. Zhang[45], X.M. Zhang[1], X.Y. Zhang[49], Xuyan Zhang[54], Y. Zhang[71], Y. Zhang[68], Y.T. Zhang[80], Y.H. Zhang[1,57], Yan Zhang[70,57], Yao Zhang[1], Z.H. Zhang[1], Z.L. Zhang[34], Z.Y. Zhang[75], Z.Y. Zhang[43], G. Zhao[1], J. Zhao[39], J.Y. Zhao[1,62], J.Z. Zhao[1,57], Lei Zhao[70,57], Ling Zhao[1], M.G. Zhao[43], S.J. Zhao[80], Y.B. Zhao[1,57], Y.X. Zhao[31,62], Z.G. Zhao[70,57], A. Zhemchugov[36,a], B. Zheng[71], J.P. Zheng[1,57], W.J. Zheng[1,62], Y.H. Zheng[62], B. Zhong[41], X. Zhong[58], H. Zhou[49], L.P. Zhou[1,62], X. Zhou[75], X.K. Zhou[7], X.R. Zhou[70,57], X.Y. Zhou[39], Y.Z. Zhou[13,f], J. Zhu[43], K. Zhu[1], K.J. Zhu[1,57,62], L. Zhu[34], L.X. Zhu[62], S.H. Zhu[69], S.Q. Zhu[42], T.J. Zhu[13,f], W.J. Zhu[13,f], Y.C. Zhu[70,57], Z.A. Zhu[1,62], J.H. Zou[1], J. Zu[70,57]

[1] *Institute of High Energy Physics, Beijing 100049, People's Republic of China*
[2] *Beihang University, Beijing 100191, People's Republic of China*
[3] *Beijing Institute of Petrochemical Technology, Beijing 102617, People's Republic of China*
[4] *Bochum Ruhr-University, D-44780 Bochum, Germany*
[5] *Budker Institute of Nuclear Physics SB RAS (BINP), Novosibirsk 630090, Russia*
[6] *Carnegie Mellon University, Pittsburgh, Pennsylvania 15213, U.S.A.*
[7] *Central China Normal University, Wuhan 430079, People's Republic of China*
[8] *Central South University, Changsha 410083, People's Republic of China*
[9] *China Center of Advanced Science and Technology, Beijing 100190, People's Republic of China*
[10] *China University of Geosciences, Wuhan 430074, People's Republic of China*
[11] *Chung-Ang University, Seoul, 06974, Republic of Korea*
[12] *COMSATS University Islamabad, Lahore Campus, Defence Road, Off Raiwind Road, 54000 Lahore, Pakistan*
[13] *Fudan University, Shanghai 200433, People's Republic of China*
[14] *GSI Helmholtzcentre for Heavy Ion Research GmbH, D-64291 Darmstadt, Germany*
[15] *Guangxi Normal University, Guilin 541004, People's Republic of China*
[16] *Hangzhou Normal University, Hangzhou 310036, People's Republic of China*
[17] *Hebei University, Baoding 071002, People's Republic of China*
[18] *Helmholtz Institute Mainz, Staudinger Weg 18, D-55099 Mainz, Germany*
[19] *Henan Normal University, Xinxiang 453007, People's Republic of China*
[20] *Henan University, Kaifeng 475004, People's Republic of China*
[21] *Henan University of Science and Technology, Luoyang 471003, People's Republic of China*
[22] *Henan University of Technology, Zhengzhou 450001, People's Republic of China*
[23] *Huangshan College, Huangshan 245000, People's Republic of China*
[24] *Hunan Normal University, Changsha 410081, People's Republic of China*
[25] *Hunan University, Changsha 410082, People's Republic of China*
[26] *Indian Institute of Technology Madras, Chennai 600036, India*
[27] *Indiana University, Bloomington, Indiana 47405, U.S.A.*
[28] *INFN Laboratori Nazionali di Frascati, (A)INFN Laboratori Nazionali di Frascati, I-00044, Frascati, Italy; (B)INFN Sezione di Perugia, I-06100, Perugia, Italy; (C)University of Perugia, I-06100, Perugia, Italy*
[29] *INFN Sezione di Ferrara, (A)INFN Sezione di Ferrara, I-44122, Ferrara, Italy; (B)University of Ferrara, I-44122, Ferrara, Italy*
[30] *Inner Mongolia University, Hohhot 010021, People's Republic of China*
[31] *Institute of Modern Physics, Lanzhou 730000, People's Republic of China*
[32] *Institute of Physics and Technology, Peace Avenue 54B, Ulaanbaatar 13330, Mongolia*
[33] *Instituto de Alta Investigación, Universidad de Tarapacá, Casilla 7D, Arica 1000000, Chile*
[34] *Jilin University, Changchun 130012, People's Republic of China*
[35] *Johannes Gutenberg University of Mainz, Johann-Joachim-Becher-Weg 45, D-55099 Mainz, Germany*
[36] *Joint Institute for Nuclear Research, 141980 Dubna, Moscow region, Russia*
[37] *Justus-Liebig-Universitaet Giessen, II. Physikalisches Institut, Heinrich-Buff-Ring 16, D-35392 Giessen, Germany*
[38] *Lanzhou University, Lanzhou 730000, People's Republic of China*
[39] *Liaoning Normal University, Dalian 116029, People's Republic of China*
[40] *Liaoning University, Shenyang 110036, People's Republic of China*
[41] *Nanjing Normal University, Nanjing 210023, People's Republic of China*
[42] *Nanjing University, Nanjing 210093, People's Republic of China*
[43] *Nankai University, Tianjin 300071, People's Republic of China*
[44] *National Centre for Nuclear Research, Warsaw 02-093, Poland*
[45] *North China Electric Power University, Beijing 102206, People's Republic of China*
[46] *Peking University, Beijing 100871, People's Republic of China*

[47] Qufu Normal University, Qufu 273165, People's Republic of China
[48] Shandong Normal University, Jinan 250014, People's Republic of China
[49] Shandong University, Jinan 250100, People's Republic of China
[50] Shanghai Jiao Tong University, Shanghai 200240, People's Republic of China
[51] Shanxi Normal University, Linfen 041004, People's Republic of China
[52] Shanxi University, Taiyuan 030006, People's Republic of China
[53] Sichuan University, Chengdu 610064, People's Republic of China
[54] Soochow University, Suzhou 215006, People's Republic of China
[55] South China Normal University, Guangzhou 510006, People's Republic of China
[56] Southeast University, Nanjing 211100, People's Republic of China
[57] State Key Laboratory of Particle Detection and Electronics, Beijing 100049, Hefei 230026, People's Republic of China
[58] Sun Yat-Sen University, Guangzhou 510275, People's Republic of China
[59] Suranaree University of Technology, University Avenue 111, Nakhon Ratchasima 30000, Thailand
[60] Tsinghua University, Beijing 100084, People's Republic of China
[61] Turkish Accelerator Center Particle Factory Group, (A)Istinye University, 34010, Istanbul, Turkey; (B)Near East University, Nicosia, North Cyprus, 99138, Mersin 10, Turkey
[62] University of Chinese Academy of Sciences, Beijing 100049, People's Republic of China
[63] University of Groningen, NL-9747 AA Groningen, The Netherlands
[64] University of Hawaii, Honolulu, Hawaii 96822, U.S.A.
[65] University of Jinan, Jinan 250022, People's Republic of China
[66] University of Manchester, Oxford Road, Manchester, M13 9PL, United Kingdom
[67] University of Muenster, Wilhelm-Klemm-Strasse 9, 48149 Muenster, Germany
[68] University of Oxford, Keble Road, Oxford OX13RH, United Kingdom
[69] University of Science and Technology Liaoning, Anshan 114051, People's Republic of China
[70] University of Science and Technology of China, Hefei 230026, People's Republic of China
[71] University of South China, Hengyang 421001, People's Republic of China
[72] University of the Punjab, Lahore-54590, Pakistan
[73] University of Turin and INFN, (A)University of Turin, I-10125, Turin, Italy; (B)University of Eastern Piedmont, I-15121, Alessandria, Italy; (C)INFN, I-10125, Turin, Italy
[74] Uppsala University, Box 516, SE-75120 Uppsala, Sweden
[75] Wuhan University, Wuhan 430072, People's Republic of China
[76] Xinyang Normal University, Xinyang 464000, People's Republic of China
[77] Yantai University, Yantai 264005, People's Republic of China
[78] Yunnan University, Kunming 650500, People's Republic of China
[79] Zhejiang University, Hangzhou 310027, People's Republic of China
[80] Zhengzhou University, Zhengzhou 450001, People's Republic of China

[a] Also at the Moscow Institute of Physics and Technology, Moscow 141700, Russia
[b] Also at the Novosibirsk State University, Novosibirsk, 630090, Russia
[c] Also at the NRC "Kurchatov Institute", PNPI, 188300, Gatchina, Russia
[d] Also at Goethe University Frankfurt, 60323 Frankfurt am Main, Germany
[e] Also at Key Laboratory for Particle Physics, Astrophysics and Cosmology, Ministry of Education; Shanghai Key Laboratory for Particle Physics and Cosmology; Institute of Nuclear and Particle Physics, Shanghai 200240, People's Republic of China
[f] Also at Key Laboratory of Nuclear Physics and Ion-beam Application (MOE) and Institute of Modern Physics, Fudan University, Shanghai 200443, People's Republic of China
[g] Also at State Key Laboratory of Nuclear Physics and Technology, Peking University, Beijing 100871, People's Republic of China
[h] Also at School of Physics and Electronics, Hunan University, Changsha 410082, China
[i] Also at Guangdong Provincial Key Laboratory of Nuclear Science, Institute of Quantum Matter, South China Normal University, Guangzhou 510006, China
[j] Also at Frontiers Science Center for Rare Isotopes, Lanzhou University, Lanzhou 730000, People's Republic of China

[k] *Also at Lanzhou Center for Theoretical Physics, Lanzhou University, Lanzhou 730000, People's Republic of China*

[l] *Also at the Department of Mathematical Sciences, IBA, Karachi 75270, Pakistan*